THE JOURNAL OF PHYSICAL CHEMISTRY C
A JOURNAL OF THE AMERICAN CHEMICAL SOCIETY

pubs.acs.org/JPCC

Article

State-Resolved Studies of OCS Scattering at the Gas−Liquid Interface: Tests of Landau—Teller/Rapp Theory for Rotational vs Vibrational Energy Transfer

Timothy A. Livingston Large and David J. Nesbitt*

Cite This: J. Phys. Chem. C 2021, 125, 22786−22796

Read Online

ACCESS | Metrics & More | Article Recommendations

ABSTRACT: Quantum-state-resolved collisional energy transfer of jet-cooled carbonyl sulfide (OCS) at the gas−liquid interface (E_{inc} = 2.2(4) kcal/mol) has been explored with a powerful combination of molecular beam scattering and high-resolution direct absorption IR spectroscopy, which has permitted the first characterization of rotational, vibrational, and transverse Doppler excitation/accommodation dynamics on a liquid for a polyatomic projectile. The results are consistent with the complete rotational and transverse translational equilibration of the incident OCS ($T_{rot,trans} \approx 10$ K) with the surface for a variety of liquids (perfluorinated polyether (PFPE), squalene, and glycerol) and liquid temperatures (T_S = 263−303 K). In dramatic contrast, however, vibrational populations in the ground (00^00), v_2 OCS bend (01^10), and ν_1 CS stretch (10^00) modes for the scattered OCS species remain far out of equilibrium with the liquid surface, indeed exhibiting adiabatic, spectator-like behavior and remaining identical (within experimental uncertainty) to vibrational temperatures observed in the incident OCS molecular beam. This spectator-like behavior for vibrational scattering clearly suggests that polyatomic vibrational coordinates must be treated separately from the other degrees of freedom, at least for low energies explored herein characteristic of the thermal desorption TD pathway. Such vibrationally decoupled behavior at energies and repulsive wall potentials sampled by the TD channel is shown to be in excellent qualitative agreement with expectations from high-level ab initio calculations and well-known Landau−Teller/Rapp vibrational energy-transfer models.

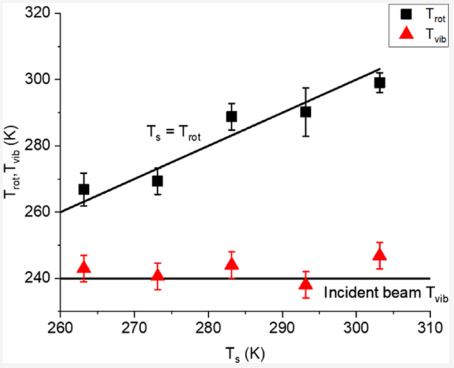

I. INTRODUCTION

Prospects for controlled engineering of chemical dynamics at the gas−liquid interface require a detailed understanding of collisional molecular energy transfer, in principle, into each of the electronic, vibrational, rotational, and translational degrees of freedom. Through a multitude of elegant chemical physics/molecular beam techniques, including direct absorption laser spectroscopy,[1,2] time of flight mass spectroscopy,[3−5] and resonance-enhanced multiphoton ionization (REMPI) plus velocity map imaging (VMI[6]) platforms, collisional energy transfer between a scattering projectile and the liquid surface has indeed been extensively explored with respect to translational and rotational degrees of freedom. In remarkable contrast to the extreme molecular heterogeneity and complexity of the gas−liquid interface, empirical evidence suggests that these scattering pathways "bifurcate" into two very much simpler channels. The first is referred to as thermal desorption (TD), whereby an incident molecule traps transiently on the surface, thermalizes completely, and then desorbs from the gas−liquid interface from a near thermal distribution of surface states. In colloquial language, such a subset of TD trajectories has "lost all memory" of the incident scattering conditions and occurs on a relatively long (>10−100 ps) time scale.[7,8] We note that this does not require final state distributions to emerge in perfect thermal equilibrium with the liquid, as there can be dynamical barriers to successful desorption that are favored/disfavored by some fraction of the internal quantum and/or translational energy states.

The second pathway is typically denoted as impulsive scattering (IS), which corresponds to molecules scattering from the gas−liquid interface while still maintaining some residual "memory" of the initial scattering condition. Stated most simply, this channel comprises all molecular flux that is *not* described by trapping desorption (TD), though Bill Hase would always remind us that unambiguous separation of these two channels is only meaningful statistically and rarely possible by inspection for a given trajectory.[9] In general, contributions to this IS channel occur on a much faster time scale (≲1−10 ps). From quantum-state-resolved molecular beam studies at

Received: July 5, 2021
Revised: September 20, 2021
Published: October 12, 2021

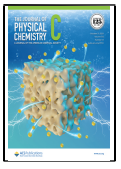

https://doi.org/10.1021/acs.jpcc.1c05993
J. Phys. Chem. C 2021, 125, 22786−22796

nonorthogonal angles of incidence, this channel often appears as a lobular forward scattering peak with a hot yet remarkably "temperature-like" distribution of internal rotational quantum states.[2,10,11] It is worth noting that the dynamical propensity toward such "hyperthermal" rotational distributions in the IS channel is far from obvious and indeed quite surprising, particularly as the translational degrees of freedom for in-plane IS scattering measured from TOF studies are routinely far out of equilibrium. Interestingly, there has been progress in characterizing the dynamical origin of these hot but "Boltzmann-esque" rotational distributions based on sharp rainbow features smoothed by thermal roughness at the gas−liquid interface. Rather remarkably, however, there have been no studies reported of any such effects in IS scattering with polyatomic molecules, including vibrational degrees of freedom, specifically vibrational excitation, deexcitation, and/or equilibration in molecular collisions at the gas−liquid interface. It is precisely this inclusion of polyatomic vibrational degrees of freedom in the gas−liquid scattering dynamics that represents the major focus of the present work.

Vibrational (V) energy transfer ($V \rightarrow R, T$) has been studied extensively in gas-phase collisions.[12−15] One central observation is that such relaxation processes for typical molecular frequencies ($\nu \approx 500-3000$ cm^{-1}) require deposition of significant ($\Delta E = h\nu \gg kT$) vibrational energy into rotation and/or translation, which in turn proceeds only via low probability collisional events.[16] These general trends are well captured by Landau−Teller theory,[17] which predicts vibrational energy transfer to be relatively inefficient and occurs only when the time-dependent force $f(t)$ between an oscillator and the collider/perturber contains significant Fourier components that match the vibrational frequency of interest. A similar trend in the predissociation dynamics[18] of van der Waals clusters was noted by Ewing and co-workers, where changes in vibrational quanta during the dissociation event are discouraged by an exponential gap law. For $V \rightarrow T$ transfer, this "exponential gap" penalty arises, from a Franck−Condon perspective, through the vanishingly small overlap between the initial vibrational state wave function and the rapidly oscillating translational wave function due to the steep repulsive van der Waals potential in the (unbound) exit channel. In more complex polyatomic species, the kinetic acceleration of vibrational excitation or relaxation arises from the presence/absence of near-resonant vibrational modes into which excess energy can be transferred from or into to accommodate this energy gap.

Investigation of vibrational energy transfer at the gas-condensed phase interface has understandably proven to be challenging.[19−30] Of special note are the pioneering studies by Wodtke and co-workers probing deexcitation of vibrationally quantum state-selected diatomic molecules colliding on single-crystal interfaces,[26−30] which have revealed two classic paradigms. If there is strong interaction/coupling of the projectile with a single-crystal metallic surface (for example, with significant ionic character due to electron transfer between metal and molecule), lifetimes are found to be short (<1 ps) and multiquantum ($\Delta\nu \gg 1$) relaxation of vibrations quite efficient.[25] For insulating single-crystal materials, on the other hand, vibrational energy-transfer efficiencies typically decrease by many orders of magnitude, revealing only modest, harmonic oscillator-like change ($\Delta\nu \approx 0, 1$) in the molecular vibrational quantum state. However, it is not simply a matter of conductive versus insulating materials, as there are also single-crystal metal−absorbate systems (e.g., Au + CO ($\nu = 1$)), for which molecular vibrations have been shown to survive for 100s of picoseconds.[28] The vibrational metastability in such systems has been attributed to anomalously weak adsorbate−surface interactions due to minimal electron transfer to/from the metal and leaving the molecule only weakly physiabsorbed. How these simple gas-surface intuitions might transfer from the long-range order of a single-crystal metal vs insulator surface to the far more disordered environment of the gas−liquid interface, however, remains essentially unexplored.

This study takes special advantage of polyatomic molecules as projectiles for study of vibrational energy-transfer dynamics at the gas−liquid interface. Carbonyl sulfide (OCS) is a particularly suitable molecular probe for such energy-transfer dynamical studies, as a linear triatomic molecule with a good balance between (i) low rotational constant ($B \approx 0.203$ cm^{-1}) and yet (ii) a very strong infrared fundamental (integrated absorption coefficient $S_0 \approx 590$ km/mol $\approx 9.8 \times 10^{-17}$ cm^2 cm^{-1}/molecule) in the CO stretch region (2050 cm^{-1}), accessible to probing with quantum cascade lasers. This combination allows for a suitably large number of final scattered rotational states ($J_{max} \approx 100$) to be readily generated via collisions at the gas−liquid interface, and yet each state still remains detectable with our present experimental sensitivity. Most importantly, linear polyatomic OCS has two low-frequency vibrational modes below 1000 cm^{-1}, specifically the ν_2 OCS bend at 520 cm^{-1} and the nominally ν_1 CS stretch at 860 cm^{-1}. As a result, both the OCS bend (01^10) and CS stretch (00^01) excited states are even weakly thermally populated in the pulsed slit valve stagnation region and, if insufficiently cooled in the supersonic expansion, can be sensitively detected in the same spectral region via CO stretch "hot bands" (e.g., ($11^10 \leftarrow 01^10$) and ($10^01) \leftarrow (00^01$)) in our laser spectrometer. Consequently, this offers a first opportunity to study in detail both (i) energy transfer from ν_1, ν_2 vibrationally excited OCS striking the liquid, as well as (ii) excitation of these same polyatomic modes by thermal and hyperthermal collisions at the gas−liquid interface. Under the low-incident-energy conditions of the present study, we find notably *inefficient* collisional energy transfer and equilibration dynamics taking place with respect to vibrational degrees of freedom, even for molecules in the trapping-desorption (TD) channel thought to have long residence times (10−100 ps) on a surface and with an enormous bath of vibrational state density available in the liquid.

The organization of this paper is as follows. A brief overview of the experimental spectrometer is described in Section II, with particular emphasis on modifications to the laser frequency diagnostics and scattering apparatus required for working with such small rotational constant and polyatomic species. In Section III, results are reported that explore *vibrational, rotational, and transverse* translational energy transfer in OCS with several prototypical liquids under low-energy beam conditions. The data highlight rapid equilibration dynamics in rotational/translational degrees of freedom, which stands in stark contrast with the extreme inefficiency and highly adiabatic nature of vibrational excitation/deexcitation dynamics. Section IV explores these results in the context of simple dynamical theories based on high level ab initio potentials for collision events, with conclusions and directions for future study summarized in Section V.

https://doi.org/10.1021/acs.jpcc.1c05993
J. Phys. Chem. C 2021, 125, 22786−22796

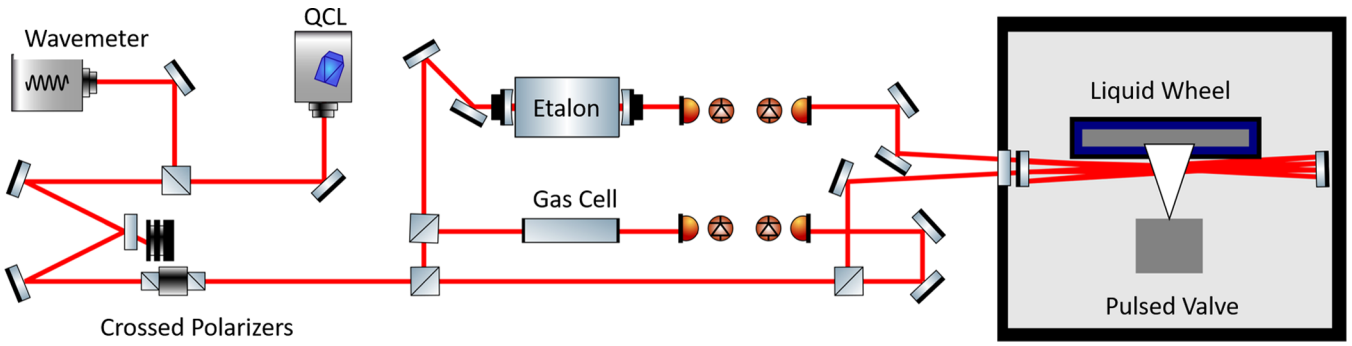

Figure 1. Experimental schematic of the continuously tunable single-mode quantum cascade laser spectrometer for quantum-state-resolved scattering at the gas−liquid interface, with details of operation described in the text.

II. EXPERIMENTAL SECTION

The gas−liquid scattering apparatus can be broken down into two major pieces: (i) the midinfrared shot-noise limited direct absorption spectrometer and (ii) the scattering vacuum chamber. Many details of this experimental apparatus have been described elsewhere and can be briefly summarized; we include herein greater focus on specific apparatus modifications relevant to the present experiments.[7,31−35] A schematic diagram of the laser optical system is shown in Figure 1. The light source is an external cavity single-mode quantum cascade laser (Daylight Solutions), capable of generating as much as ∼300 mW of single-mode infrared light from ∼2000 to 2200 cm^{-1} with a spectral line width of ∼10 MHz. Since this significantly exceeds the linear regime of our IR photodetectors, the laser IR power is first reduced 50× by weak reflection from a tilted BaF window and then smoothly trimmed to the desired level by a pair of crossed Rochon polarizers. After transmission through the rest of the optical system and vacuum scattering chamber, this results in ∼10−30 μW on each of two LN_2 cooled InSb photovoltaic (signal and reference) detectors.

This high-resolution light source is characterized by three nested stages of frequency diagnostics. We first utilize a Michelson wavemeter (Bristol wavemeter 621b) to obtain a rough estimate ($\Delta\nu \approx 0.01$ cm^{-1}) of the absolute start scan frequency. Second, transmission signals through a room-temperature OCS gas cell (500 mT, 1−5 cm path length) are recorded in parallel during the automated scan, which in conjunction with the wavemeter reading and a Fourier transform IR (FTIR) OCS atlas (with 0.00001 cm^{-1} precision and accuracy) permits unambiguous confirmation of this start frequency. Finally, we monitor transmission fringes through an off-axis Fabry−Perot (bowtie) etalon with a finesse of ∼20−30 and 250 MHz FSR, generating a convenient ruler with which to interpolate and provide a linear scan axis. Sample spectral diagnostics through the transmission cell and Fabry−Perot etalon are represented in Figure 3, which indicate the presence of a strongly optically saturated absorption line in the CO stretch fundamental band ($(10^00) \leftarrow (00^00)$, R(17)), with additional weaker lines corresponding to hot band transitions out of the doubly degenerate OCS bend ($(11^10) \leftarrow (01^10)$, R(39)), split into a e/f parity doublets by l-doubling in $\nu_1 = 1$ lower/upper levels. Note also the corresponding weaker triplet absorption features marked with asterisks, which arise from $OC^{34}S$ bands in the fundamental $\nu_3 = 1 \leftarrow 0$ CO stretch and readily observable in natural isotopic abundance (4%).

Finally, the reduced IR light is split into signal and reference beams, with the distribution of OCS rovibrational quantum states in the vacuum chamber probed via transient absorption of the quantum cascade laser signal light in a 16 pass Herriot cell. The probe laser multipass axis is oriented parallel to the rotating wheel and perpendicular to the scattering plane, 1 cm away from the liquid surface and ∼2 cm along the surface from the location where the center of the molecular beam hits, which puts the measurement region at 65° away from the surface normal. The transmitted IR light is measured exploiting fast (10 MHz) balanced detection electronics on a pair of matched IR photodetectors, with one of the two detection arms traversing the vaccum chamber Herriot multipass cell. The net result is a differential absorbance sensitivity of $<1 \times 10^{-5}$ in the experimental detection bandwidth (∼1 kHz), which for OCS scanning in $N \approx 10$ steps over a single line translates into a minimum detectable concentration of $\rho_{min} \sim 10^7/cm^3$/quantum state.

The gas−liquid scattering events occur in a 60 L Al vacuum chamber, evacuated by a 6 inch diffusion/roughing pump. In the presence of the molecular beam gas pulse, the chamber pressure remains below 10^{-4} Torr, which ensures collision-free mean path lengths several times the physical dimensions of the vacuum chamber. The scattering system is made up of a molecular beam source, the scattering target, and the multipass cell. The beam source is of the Proch and Trickl design,[36] with a mixture of 5% OCS/95% argon expanded through a 0.508 mm diameter orifice at a stagnation pressure of $P \sim 80$ Torr. These low pressures are chosen intentionally to achieve sufficiently cold rotational temperatures yet prevent clustering of OCS into dimers, trimers, etc., as confirmed by linear curves of growth vs pressure for OCS transitions observed in the incident beam. The average speed in the molecular beam pulse is $v_0 \approx 5.50(50) \times 10^4$ cm/s, directly measured by a simple time of flight setup as a function of microphone displacement. This translates into an incident OCS energy of 2.2(4) kcal/mol for collisions with the liquid surface, with the molecular beam in a vertical plane, striking the surface from below, and oriented at a 65° polar angle with respect to the liquid normal. This means the measurement region is sensitive to molecules that back scatter from $\theta \approx -40$ to nearly $\theta \approx 90°$ forward scattering, with peak sensitivities at $\theta \approx +70°$ away from normal. The transverse distribution of translational velocities in the incident beam is constrained by a 3 mm diameter on-axis skimmer situated 25 mm from the nozzle orifice, which achieves a half cone angle of 3.8°.

By the way of assessment of rotational/vibrational cooling in the supersonic expansion, we directly monitor the CO stretch

https://doi.org/10.1021/acs.jpcc.1c05993
J. Phys. Chem. C 2021, 125, 22786−22796

spectrum of OCS of the incident molecular beam. As shown in Figure 3 (lower panel), there are clearly visible contributions from thermally populated "hot band" transitions out of both the low-lying OCS bend (01^10) and CS stretch (00^01) excited states, in addition to the much more highly populated ground (00^00) state. From Boltzmann analysis of *rotational* populations in each of the three lower vibrational states, we can infer a characteristic temperature of $T_{rot} \approx 10$ K. However, an equivalent Boltzmann analysis of *vibrational* populations summed over each rotational manifold corresponds to $T_{vib} \approx 240(5)$ K, which is clearly out of equilibrium with $T_{rot} \approx 10$ K rotational temperatures in the supersonic expansion. Such nonequilibrium behavior between rotational/vibrational degrees of freedom is not uncommon[15] and arises from the much larger number of collisions required to cool vibrations in a supersonic pinhole expansion, essentially due to the much larger vibrational (10^2-10^3 cm^{-1}) vs rotational (10^0-10^1 cm^{-1}) energies that need to be collisionally removed. Indeed, this provides a first indication of "frustrated" vibrational energy-transfer dynamics in the throat of a pinhole supersonic expansion, establishing a crucially important baseline for interpreting the subsequent collision dynamics at the gas−liquid interface.

The liquid target for these scattering studies is based on a temperature-dependent rotating wheel setup described in ref 7. The liquid scattering surface is prepared according to the method of Lednovich and Fenn,[37] using a rotating (∼0.2 Hz) bead blasted stainless steel wheel (12.7 cm diameter) half submerged in a copper reservoir of liquid and scraped with a stationary razor blade to present a thin (∼500 μm), freshly prepared gas−liquid interface to the incident molecular beam. The liquid reservoir and gas−liquid surface are thermally isolated from the rest of the vacuum chamber by Teflon spacers, with liquid-surface temperatures stabilized by a two-stage servo loop cooling apparatus. Specifically, coarse thermal cooling/heating of the liquid is achieved by recirculating ethanol refrigerant, with fine temperature control via a thermoelectric element on the backplate, which in turn is servo loop stabilized ($\Delta T \approx 0.01$ K) to a thermistor epoxied to the front of the copper trough.

This study investigates three different classes of liquids that sample different scattering dynamical regimes: (1) perfluorinated polyether (PFPE, Krytox 1506, (F-[$CF(CF_3)$-CF_2O]$_{14(avg)}$-CF_2CF_3)), as a prototype for a rough but chemically inert liquid surface, (2) squalane (2,6,10,15,19,23-hexamethyltetracosane, $C_{30}H_{62}$), as a prototype for fully aliphatic, strongly hydrophobic surface, and (3) glycerol (1,2,3-propanetriol, $C_3H_8O_3$), as a prototype for a much more hydrophilic surface due to multiple protruding OH groups. Each liquid is degassed under ∼1 mTorr vacuum at room temperature for several hours to remove dissolved atmospheric gases or at slightly elevated temperatures (∼ 350 K) for glycerol liquid studies to allow for complete degassing within a reasonable (12 h) time frame.

Quantum-state (v,J) and Doppler-resolved ($\Delta\nu_{transverse}$) signals for the scattered OCS are measured in a 16 pass concentric Herriot cell with a single-pass cell length of ∼40 cm. As can be seen in Figure 1, this beam multipass lies parallel to the liquid-surface plane and perpendicular to the molecular beam. This ensures that Doppler broadening in transitions reports on velocity distributions transverse to the scattering plane formed by the molecular beam and liquid-surface normal. One particularly crucial addition to the scattering setup is an LN_2-cooled cold trap at the top of the vacuum chamber, which achieves surface-operating temperatures down to 90 K and helps freeze out background OCS in the vacuum chamber. Since the QC laser line width (∼10 MHz) is an order of magnitude lower than the Doppler FWHM of a typical room-temperature OCS transition (∼100 MHz), there is negligible amplitude noise contribution arising from frequency-jitter transmission on scattered molecules. However, there can be significant frequency-induced amplitude fluctuation due to thermal background OCS gas present in much higher concentrations. As this frequency noise appears only on the signal detector, it circumvents subtraction circuit band pass filters and appears as unsubtractable, *noncommon mode* amplitude noise. Fortunately, this noise source is effectively eliminated by LN_2 cryopumping to reduce the OCS background gas by ∼10−100-fold, which in turn reduces frequency-induced amplitude noise by a proportionate amount.

Experimental data acquisition procedure consists of computer-controlled digitization of time-domain traces monitoring the the scattered OCS gas pulse event (2000 μs) as a function of laser frequency (adjustable step size: $\Delta\nu$ = 3−7 MHz) tuning over the full 2050 to ∼2100 cm^{-1} spectral window. This broad 50 cm^{-1} scan range is broken down into smaller computer-controlled continuous scans of ∼0.8 cm^{-1}, with an approximately 0.1 cm^{-1} overlap between each segment to eliminate spectral gaps. The time traces at each laser frequency are converted into absorbance A(ν) by integrating over the rising edge (300 μs) of the gas pulse, subtracting an equivalent integrated baseline (300 μs) window before the gas pulse, scaling the transmitted signal by incident light level and expressing as a base e logarithm. The relative frequency axis for each scan segment is obtained by linear interpolation between etalon peaks, with zeroth-order absolute frequency estimates from the IR wavemeter. Such wavemeter IR readings contain small systematic offsets (of order $\Delta\nu \approx 0.03$ cm^{-1}) but are nevertheless sufficiently accurate to make an unambiguous match with a room-temperature reference cell OCS spectrum, which in turn provides accurate *absolute* frequencies by comparison with a high-precision HITRAN database.[38] Sample reference cell and etalon traces are shown in Figure 2, which displays a small 6 GHz (0.2 cm^{-1}) blow-up region. The net result is access to an information-rich, high-resolution spectral scan (with 150 000−350 000 elements) covering the entire R branch region and much of the P branch region for the CO stretch fundamental ($(10^00) \leftarrow (00^00)$) and bending/CS stretching "hot bands" ($(11^10) \leftarrow (01^10)$, $(10^01) \leftarrow (00^01)$) out of the ground ($00^00$) and lowest two vibrationally excited states ((01^10), (00^01)).

III. RESULTS AND ANALYSIS

Extraction of the quantum-state-resolved column-integrated molecular densities is obtained by a global fit of the high-resolution scattering spectra,[39] with a sample fit region displayed in Figure 4. The analysis is based on a least-squares fitting of a population model using HITRAN transition frequencies to fit the entire spectrum. The spectral model is based on several reasonable assumptions. (i) First of all, the upper CO stretch (v,J) state sampled in each spectroscopic transition is unpopulated, with rovibrational energies ∼2000−3000 cm^{-1} above the ground (00^00) state and completely inaccessible at low collision energies explored. (ii) Second, high-resolution line shapes for each transition are Doppler limited and arise from a Gaussian distribution of transverse

https://doi.org/10.1021/acs.jpcc.1c05993
J. Phys. Chem. C 2021, 125, 22786−22796

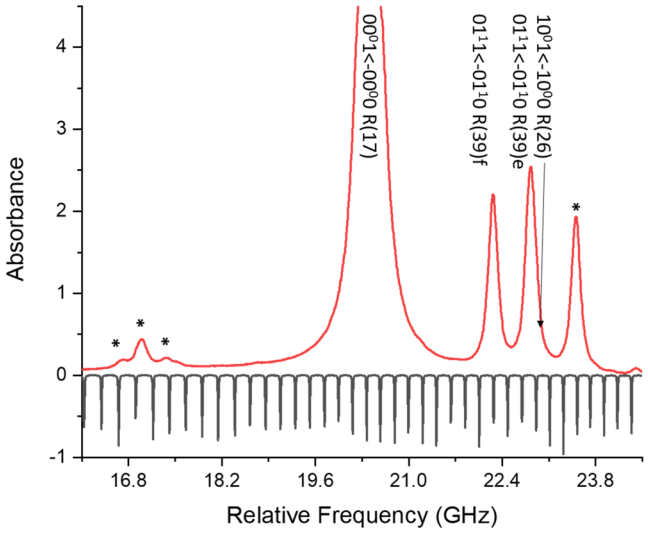

Figure 2. Experimental frequency diagnostics: The etalon trace and thermal OCS reference gas cell (50 Torr) allow for absolute frequency and precise relative frequency calibration (* marks lines from the less-abundant $^{16}O^{12}C^{34}S$ isotopologue).

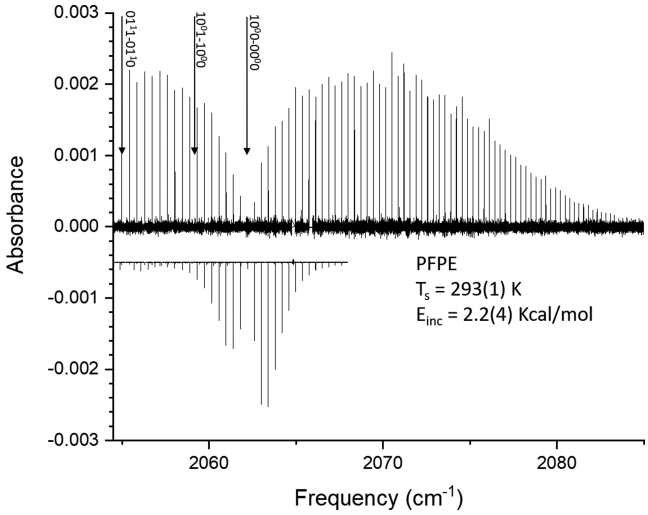

Figure 3. Sample continuous single-mode QCL IR laser scan of OCS scattering from PFPE at E_{inc} = 2.2(4) kcal/mol. The downward peaks in the lower half panel represent an absorption spectrum of the rotationally much colder ($T_{rot} \approx 10$ K) incident molecular beam.

velocities common to all v,J lower states. (iii) In this limit, the experimental spectrum can be expressed as the following linear superposition

$$A(n_j) = \sum_i S_i(n_j)^* P_i \quad (1)$$

where P_i are column-integrated densities (#/cm^2/quantum state) in the lower state i and S_i (n_j) is the calculated cross-section (cm^2/#) from state i as a function of laser frequency n_j. The integrated cross sections for each line are obtained from the HITRAN library, with only transitions from the two most common isotopologues $^{16}O^{12}C^{32}S$ (≈94%) and $^{16}O^{12}C^{34}S$ (≈4%) considered. From linear least-squares fits of this model to the experimental spectrum, the column-integrated molecular densities (P_i) can be extracted. In these linear fits, we have limited J rotational states to those with $E_{rot} > 100$ cm^{-1} ($J \geq 22$) due to both residual incident beam contamination and finite levels of OCS gas background along the 16 × 40 cm laser absorption path inside the vacuum chamber. The high quality of fit is evident in Figures 3 and 4, in particular with the precision of frequency alignment and line shape modeling robustly obvious in the spectral blowup in Figure 4.

The column-integrated densities extracted from this least-squares spectral model for OCS scattering data at E_{inc} = 2.2(4) kcal/mol from PFPE (T_S = 293 K) are summarized in Figure 5. In addition to extensive collisional energy transfer into a broad distribution of rotational levels (e.g., up to J = 67 with E_{rot} = 1095 cm^{-1}), the data clearly also reveal significant column-integrated densities in both the ground (00^00) and the two lowest vibrational manifolds (01^10), (10^00). Closer inspection reveals that each of these rovibrational manifolds appears "temperature-like" and can be well fit with a simple rotational Boltzmann distribution, as illustrated by straight-line fits in Figure 6. Indeed, manifolds exhibit indistinguishable rotational temperatures within experimental error, with slopes corresponding to $T_{rot,gnd\ state}$ = 290(7) K $T_{rot,OCS\ bend}$ = 297(20) K, and $T_{rot,CS\ stretch}$ = 310(100) K for the ground, OCS bend, and CS stretch excited modes, respectively. As these three distributions are experimentally identical, an Occam's razor perspective motivates a constrained analysis as one common rotational manifold. By way of additional support, such a constrained fit yields T_{rot} = 298(5) K, which is in excellent agreement with the T_S = 294(1) K experimental liquid temperature. Simply summarized, the data in each of the three vibrational manifolds suggests complete rotational thermalization to T_S at the lowest molecular beam collision energies (E_{inc} = 2.2(4) kcal/mol) explored herein. From detailed balance considerations, such behavior is consistent with unity sticking into the trapping-desorption channel (TD) for all rotational states significantly populated in the incident beam, as confirmed previously in a number of gas−liquid molecular projectile scattering systems.[40]

However, of particular dynamical interest and the explicit focus of the present work is a first glimpse at the *vibrational distribution* of final states in the scattered OCS flux. Specifically, we sum over all rotational states and can report total populations in each of the three vibrational manifolds. Despite only a limited number of vibrational data, these populations (in red) fall quite nicely on a linear Boltzmann plot, which is consistent with a vibrational temperature of T_{vib} = 240(5) K. Particularly noteworthy in Figure 7 is the comparison with the three-point plot (in blue) for relative vibrational populations in the incident molecular beam, which is not quite as linear yet closely matches the corresponding Boltzmann slopes for the scattered populations (in red). This striking degree of parallelism makes clear that there is little if any substantive change in OCS vibrational populations before and after a collision with the gas−liquid interface. Therefore, the highly nonequilibrium rovibrational cooling dynamics in the supersonic expansion (i.e., $T_{rot} \approx 10$ K $\ll T_{vib} \approx 240(5)$ K) is largely recapitulated in the scattered OCS flux, but now with (i) the rotations *warming rapidly up to* and yet (ii) vibrations in our polyatomic projectile remaining substantially *colder than* the liquid-surface temperature, T_S (i.e., $T_{rot} \approx 298(5)$K > $T_{vib} \approx$ 250(5) K). Simply stated, the vibrational degrees of freedom in the OCS projectile remain weakly coupled with the liquid interface, which speaks to a high degree of vibrational adiabaticity in the gas−liquid collision dynamics. Though such a propensity for vibrational adiabaticity is well appreciated

https://doi.org/10.1021/acs.jpcc.1c05993
J. Phys. Chem. C 2021, 125, 22786−22796

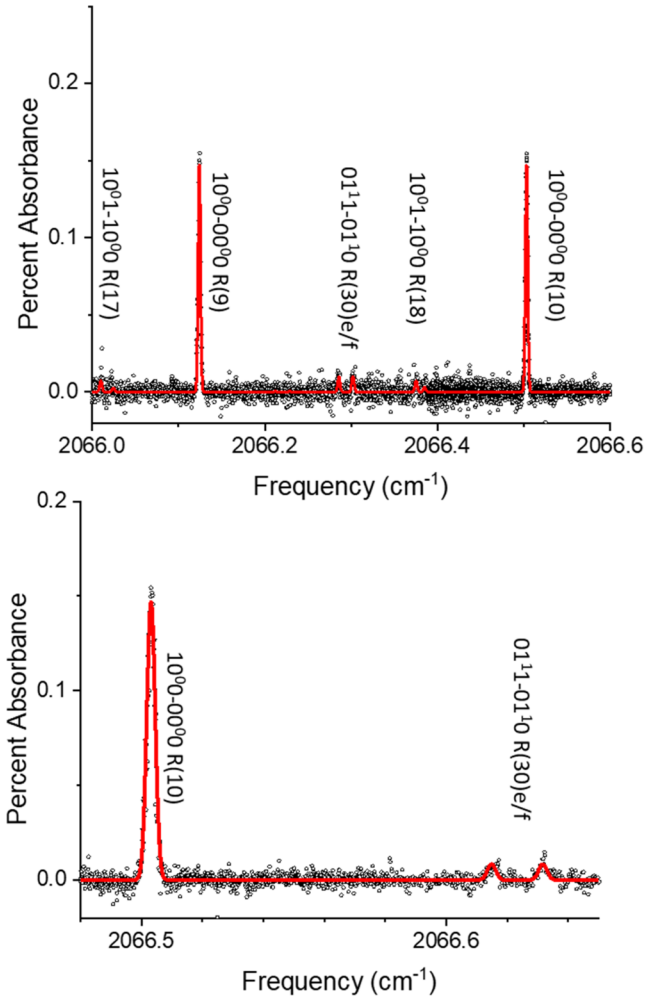

Figure 4. High-resolution blowup (≈0.6 cm^{-1} region) of the sample single-mode spectrum (see Figure 3) for OCS scattering from the gas−PFPE liquid interface (black open circles), with the least-squares fit model spectrum (solid red line). The rms absorbance noise in the further expanded lower panel (≈0.15 cm^{-1} scan region) is 2.3×10^{-5} in the detection bandwidth, which is within a factor of 2 of the quantum-shot-noise limit.

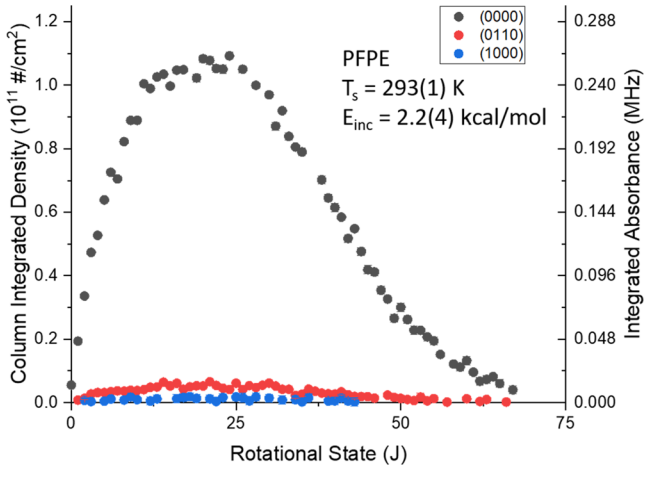

Figure 5. Rotational populations in ground (00^00), OCS bend excited (01^10), and CS stretch excited (10^00) states, as extracted from linear least-squares fits of the scattered OCS spectra to a HITRAN line simulation. The liquid is PFPE at T_S = 293(1) K.

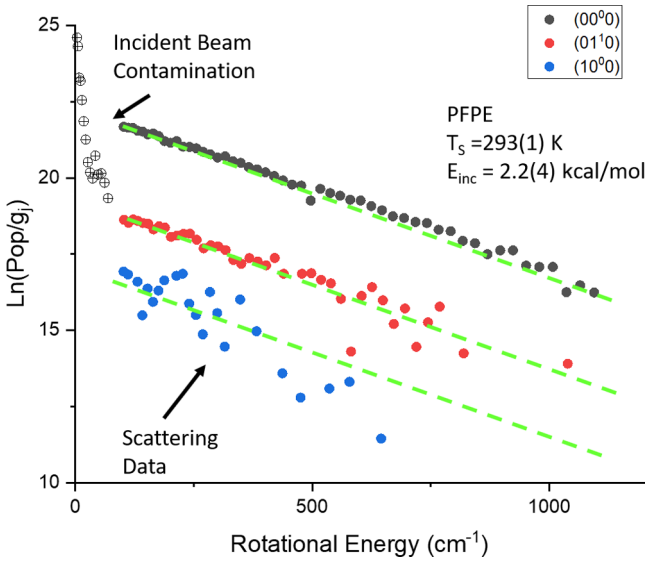

Figure 6. Rotational Boltzmann plot, indicating J state distributions with parallel straight-line slopes that reflect thermal populations fully equilibrated with the PFPE liquid (T_S = 293(1) K).

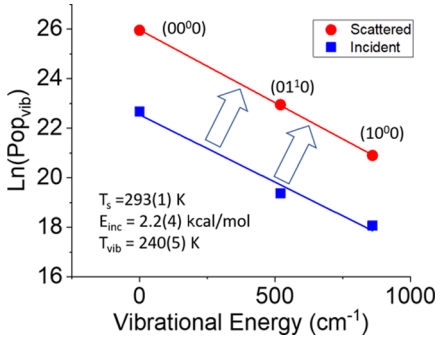

Figure 7. Vibrational Boltzmann plot of both the incident beam (blue) and scattered OCS molecules (red). Interestingly, the measured OCS vibrational populations (solid lines) are "Boltzmann-esque" (i.e., temperature-like) in nature and correspond to temperatures (T_{vib} = 240(5) K) notably cooler than the gas−liquid interfacial temperature (T_S = 293(1) K) and yet also far hotter than rotational temperatures achieved in the supersonic molecular beam (T_{rot} = 10(2) K).

for gas-phase collisions,[15] the corresponding trend for collisions on liquids is far less evident, with the present data on OCS scattering representing, to the best of our knowledge, the first direct evidence for such weak vibrationally inelastic collision dynamics at the gas−liquid interface.

One could reasonably argue that this behavior depends sensitively on the explicit nature (e.g., polar, nonpolar, etc.) of the molecule−liquid intermolecular potential. To address this possibility, we have supplemented the above data with OCS scattering (E_{inc} = 2.2(4) kcal/mol) on the surfaces of two other low-vapor-pressure liquids commonly studied in the gas−liquid scattering literature, specifically squalane (van der Waals, hydrophobic) and glycerol (hydrogen bonded, hydrophilic). Spectral fits and population analysis for these additional liquids proceed identically to that of PFPE scattering, again yielding fully thermalized rotations and yet highly *nonequilibrium* vibrational distributions, with fitted rotational and vibrational temperature results for all three liquids summarized in Figure 8. Within 1σ experimental uncertainties, all three liquid

https://doi.org/10.1021/acs.jpcc.1c05993
J. Phys. Chem. C 2021, 125, 22786−22796

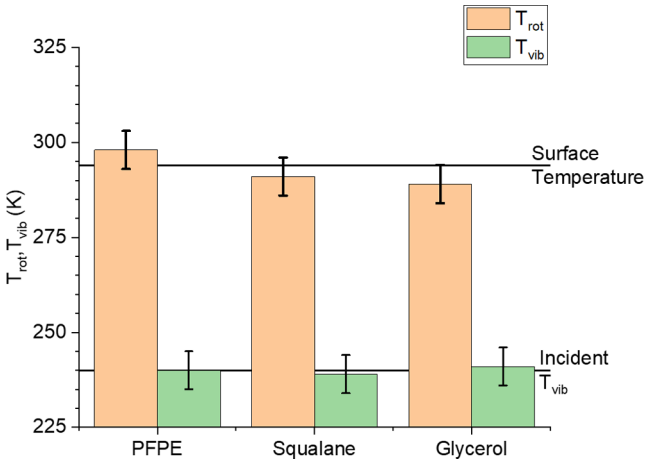

Figure 8. Summary of OCS scattering results at E_{inc} = 2.2(4) kcal/mol for OCS collisions from multiple liquids in multiple liquid reservoirs. Note that rotational temperatures are all in reasonably good agreement with the liquid-surface temperature (T_S), while vibrational temperatures are dramatically colder than T_S and indeed much closer to the values established in the incident molecular beam.

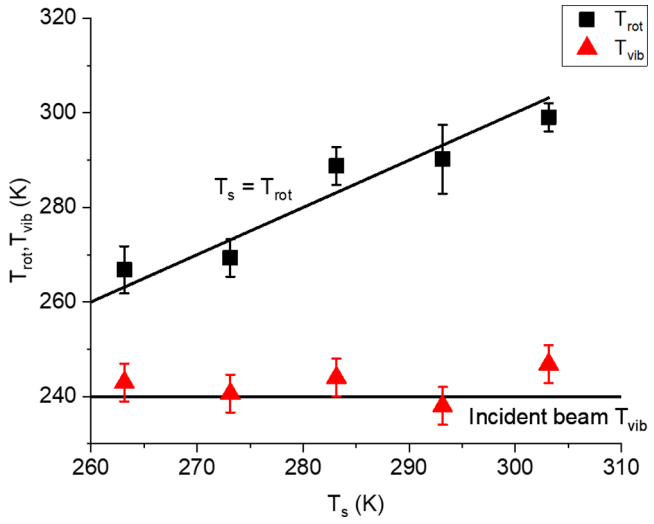

Figure 9. Dependence of rotational (T_{rot}) vs vibrational (T_{vib}) degrees of freedom in the scattered OCS flux on liquid-surface temperature (T_S). Note that T_{rot} is equilibrated and scans smoothly with T_S, whereas T_{vib} is much colder than but remarkably independent of the liquid temperature.

systems indicate identical behavior with respect to rotational thermalization (T_{rot}) to the surface temperature (T_S). In remarkable contrast, however, the data for each of the three liquids reveal no measurable change in scattered OCS vibrational temperature (T_{vib}) with respect to the incident molecular beam. One must therefore conclude that the time scale for OCS vibrational equilibration is in significant excess of the time scales for collisional interaction at the gas−liquid interface, at least for room-temperature liquids and at these low collision energies.

This striking *nonequilibration* of OCS vibrations for low-energy TD collisions at the gas−liquid interface, despite clear evidence for complete equilibration of both rotational and translational degrees of freedom, deserves further inspection. As an ancillary set of experiments, therefore, low-energy TD scattering studies have been repeated for OCS scattering from PFPE liquid as a function of liquid-temperature conditions from T = 263 to 303 K. Specifically, OCS rotational populations in each of the three vibrational manifolds ((0000), (01^10), (1000)) have been subjected to the same constrained Boltzmann analysis to yield a common T_{rot}, with the total populations summed in each manifold to yield vibrational distributions and similarly fitted to yield values of T_{vib}. The resulting dependence of T_{vib} and T_{rot} on the liquid PFPE temperature (T_S = 263−303 K) is summarized in Figure 9 and reveals several trends worth highlighting.

First of all, OCS at low collision energies clearly rotationally thermalizes and fully equilibrates with the gas−liquid interface, with T_{rot} smoothly tracking the surface temperature ($T_{rot} \approx T_S$). In contrast, the corresponding *vibrational temperatures* for OCS are completely insensitive and essentially flat with respect to warming of the liquid interface (T_S). Furthermore, these OCS vibrational temperatures are all slightly below that of the 300 K gas in the stagnation region, consistent with weak cooling of polyatomic vibrational degrees of freedom in the supersonic expansion, and yet essentially no further excitation or deexcitation dynamics in subsequent collisions at the gas−liquid interface. Alternatively stated, the measured vibrational temperatures are all within experimental error of the corresponding temperature distributions in the incident beam, indicating a lack of coupling between OCS vibrations and the liquid PFPE interface, despite there being sufficient time to achieve complete equilibrium with respect to rotational/translational degrees of freedom. In summary, at all temperatures and collision energies sufficiently low enough to achieve complete trapping desorption (TD) and thus equilibration in rotation and translation, low-lying vibrations in polyatomic OCS appear to behave as vibrational spectators in the gas−liquid scattering event.

IV. DISCUSSION

The current study presents, to the best of our knowledge, first results for vibrationally quantum-state-resolved scattering of a polyatomic molecule at the gas−liquid interface, which has permitted probing of thermal accommodation dynamics with respect to (i) rotational, (ii) translational, and (iii) vibrational degrees of freedom. The essential result is that rotational/translational degrees of freedom in the OCS/Ar molecular beam are strongly cooled by the supersonic expansion ($T_{rot} \approx$ 10 K) and then rapidly thermalize ($T_{rot} \approx T_{trans} \approx T_S$) in single low-energy collisional interactions at each of three gas−liquid interfaces and all temperatures sampled. In clear contrast, however, distributions in the lowest three thermally populated vibrational states (00^00, 10^00, 01^10) are only very weakly cooled in the supersonic expansion ($T_{vib} \approx$ 230K) and remain essentially completely unequilibrated in subsequent collisions with the three liquid surfaces (PFPE, squalene, glycerol) investigated.

To gain additional insight into the origins of such nonequilibrium effects, we consider predictions based on simple models of collisional energy transfer. At the outset, we note that such behavior can be qualitatively rationalized from Fermi's Golden rule. In the framework of such a Fermi Golden rule theory, the rate constant for collisional mixing between asymptotic rovibrational quantum states Ψ_i and Ψ_j is predicted to be

$$k_{i\to j} = 2\pi/\hbar\, |\langle \Psi_i | V_{int} | \Psi_j \rangle|^2 \rho(E_j) \quad (2)$$

https://doi.org/10.1021/acs.jpcc.1c05993
J. Phys. Chem. C 2021, 125, 22786−22796

where $|\langle\Psi_i|V_{int}|\Psi_j\rangle|$ is the off-diagonal matrix element of the interaction potential and $\rho(E_f)$ the local density of final states. For perturbative energy transfer ($\Delta E \ll E_{inc}$) and slowly varying level spacings, this local state density $\rho(E_j)$ is approximately $1/\Delta E$, from which one can immediately recast the rate constant in terms of simple second-order perturbation theory, i.e.,

$$k_{i\to j} = 2\pi/\hbar\,|\langle\Psi_i|V_{int}|\Psi_j\rangle|^2/\Delta E_{ij} \tag{3}$$

For the case of pure *rotational transfer* where adjacent energy differences are small ($\Delta E_{ij} \approx 2B_{OCS}\,J \ll E_{inc}$), it takes only relatively weak collisional interactions to mix these states, therefore predicting facile thermal equilibration at the gas−liquid interface. This is fundamentally different from the dynamical behavior anticipated for *vibrational* degrees of freedom in OCS, which have 3 orders of magnitude larger energy spacings ($\Delta\nu_{OCS\ bend}$ = 520 cm^{-1}, $\Delta\nu_{CS\ stretch}$ 860 cm^{-1}) and would therefore suggest much stronger collisional interactions required to excite/deexcite/thermalize the polyatomic OCS state distributions. Interestingly, although vibrational spacings are now actually comparable to the incident collision energy (E_{inc} = 2.2(4) kcal/mol = 770(140) cm^{-1}) and thus outside of the realm of simple perturbation theory, eq 2 nevertheless qualitatively rationalizes our experimental observation of highly inefficient energy transfer into/out of the polyatomic vibrational degrees of freedom. Indeed, due to the limited number of collisions in a supersonic jet (e.g., $N_{coll} \approx$ 100−200 at P_{stag} = 100 Torr, d = 0.5 mm), this simple Fermi Golden rule model provides motivation for both (i) poor vibrational cooling down from T_{stag} in the pinhole supersonic expansion and (ii) inefficient thermal equilibration of these high-frequency polyatomic vibrational modes in subsequent collisions with the gas−liquid interface. Two questions of key interest are simply (i) how inefficient is this process and (ii) what do these experimental observations imply for interaction time scales in a typical trapping-desorption (TD) event?

We can put these nonequilibrium predictions on a more quantitative footing by calculating the *ab initio* interaction potential for OCS collisions with the PFPE surface. To keep things simple, we follow the procedure of Hase and co-workers in developing atom−atom potentials for CO_2 scattering from fluorinated self-assembled monolayers (FSAMs). Specifically, we calculate one-dimensional (1D) potential energy curves for each of seven different approach geometries for OCS colliding with a carbon tetrafluoride molecule (CF_4) by way of proxy for a highly fluorinated liquid interface. At each intermolecular geometry and distance, high-level *ab initio* MOLPRO calculations have been performed[12] at the CCSD(T)-f12 level, based on explicitly correlated (f12) electron methods and correlation consistent Dunning basis sets (AVnZ-f12; n = 2, 3, 4). Additionally, we also perform standard counterpoise corrections for basis set superposition error (BSSE) and extrapolate our results to the complete basis set limit (CBS), using different recommended extrapolation exponents of Peterson and co-workers for both the reference and correlation energies. The seven 1D geometries are chosen to sample the strongest possible interactions between our effective liquid surface and polyatomic projectile, with sample results from two such 1D approach geometries (top panel, OCS coplanar with the FCF moiety; bottom panel, OCS collinear with the CF bond) captured in Figure 10. Least-squares fits of these 1D potentials to a simple Morse parametrization predict well

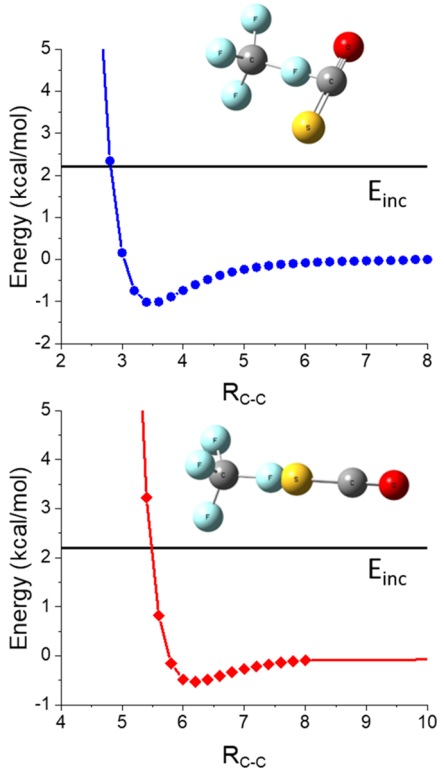

Figure 10. Sample OCS−CF_4 molecular approaches for high-level ab initio MOLPRO CCSD(T)-f12/PVnZ-f12 (n = 2, 3) CBS calculations. The top and bottom curves represent the most physically relevant approach geometries for vibrational excitation of the OCS bend and CS stretch modes, respectively.

depths on the order of $D_e \approx$ 0−1 kcal/mol, with a characteristic exponential repulsive wall parameter of roughly $\alpha \approx 2$/Å.

As an early gold standard in collisional $T \to V$ energy-transfer theory, a near analytic quantum model was developed by Landau and Teller, whereby a structureless atom A collides with a collinear diatomic BC via an exponentially repulsive potential $V_{1D}(x) = V_0 \exp(-\alpha x)$. The three key model assumptions are (i) harmonic vibrations, (ii) linearized coupling in the differential displacement of proximate atoms, and (iii) collisional time scales (τ_{coll}) much longer than the vibrational period (τ_{vib}). Based on these assumptions, Landau and Teller were able to derive quantum mechanical perturbative collision excitation probabilities from v = 0 → 1 of the form[41]

$$P_{0\to 1} \sim \exp\left(-\frac{2\pi\omega}{\alpha v_0}\right) \tag{4}$$

where ω is the angular frequency (radians/s) of the diatomic vibration under study, α is the exponential repulsion potential parameter, and v_0 is the asymptotic approach velocity. While the prefactor in eq 4 proves difficult to be calculated quantum mechanically, one can estimate it from a closely related semiclassical derivation by Rapp for collinear A + BC(v'') → A + BC(v') collisional excitation.[42] Specifically, Rapp extended Landau−Teller theory results to show that the v = 0 → 1 semiclassical transition probability can be analytically written as

https://doi.org/10.1021/acs.jpcc.1c05993
J. Phys. Chem. C 2021, 125, 22786−22796

$$P_{0\to 1} = 8\pi^2 \frac{\omega}{\hbar\, a^2} \frac{\mu_{A,BC}^2}{\mu_{BC}} \frac{M_C^2}{(M_B + M_C)^2} e^{-2\pi\omega/v_0 a} \quad (5)$$

for which $\mu_{A,BC}$ and μ_{BC} represent the reduced masses of A + BC and BC, respectively, with m_B and m_c as proximate and distal diatomic atoms, respectively. To apply such a simple diatomic model to the more complex polyatomic OCS projectile requires additional modification of eq 5 to take into account the (i) effective normal mode masses and (ii) overlap of the proximate atom B displacement onto the vibration coordinate of interest. For the present estimation purposes, it will suffice to treat the ν_3 mode as a "local" OC-S stretch with effective diatomic masses $M_B \approx M_{Sulfur}$ (32 amu) and $M_C \approx M_{Carbon} + M_{Oxygen}$ (28 amu) and similar considerations for the "local" ν_2 bending mode dominated by the motion of the central C atom resulting in $M_B \approx 12$ amu and $M_C \approx M_{Sulfur} + M_{Oxygen} = 48$ amu. Furthermore, we can expand the Morse potential as locally linear in atom displacement and replace the exponential repulsion parameter by the logarithmic derivative $\alpha = \partial \ln[V_{Morse}]/\partial r$, evaluated at the classical turning point of closest approach, i.e., at $V_{Morse}(r) \approx E_{inc}$. From Morse potential fits to both of the approach geometries shown in Figure 10, one finds the effective exponential repulsion parameter to be $\alpha \approx 6(1)$/Å at $E_{inc} \approx 2.2(4)$ kcal/mol and $v_0 \approx 5.5 \times 10^4$ cm/s, which translates into dimensionless exponents of $(2\pi\omega/v_0\alpha) \approx 18.7$ and 30.9 for the bend and CS stretch, respectively.

The resulting theoretical predictions for the $P_{0\to 1}$ inelastic collision probability vs the exponent $2\pi\omega/\alpha v_0$ are plotted in Figure 11, with highlighted points corresponding to the (ν_1)

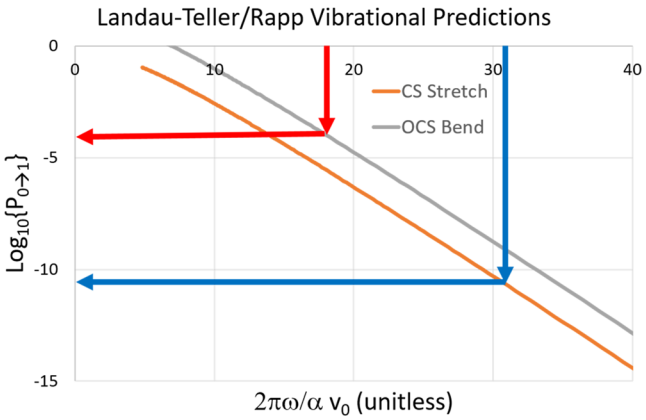

Figure 11. Landau–Teller/Rapp semiclassical modeling of $T \to V$ vibrational excitation probabilities vs the unitless velocity-dependent exponential. Gray and orange curves represent prediction for the OCS bend (ν_2) and CS stretch (ν_3) behavior, respectively.

CS stretch and (ν_2) OCS bend excitation. Although such a single collision model obviously does not account for long-lived interactions/multiple encounters with the gas–liquid interface, the reciprocal probability ($1/P_{0\to 1} = Z$) represents a first-principles estimate for the number of such low-energy collisional interactions Z required for equilibration of a given vibrational degree of freedom in OCS with T_S. For $E_{inc} \approx 2.2(4)$ kcal/mol and $v_0 \approx 5.5 \times 10^4$ cm/s, this semiclassical model translates into $Z_2 \approx 10^4$ and $Z_1 \approx 10^{11}$ for the ν_2 (01^10) OCS bend and ν_1 (10^00) CS stretch, respectively. If we consider *ab initio* interaction potentials with 3–4 Å range and atoms moving at thermal speeds (3×10^4 cm/s), a typical low-energy "single collision" event at the gas–liquid interface would be predicted to last roughly 1 ps. In conjunction with the above collision number estimates, this would imply equilibration time scales of order 10 ns even for the low-frequency OCS bend, which is already >300-fold longer than the typical mean TD interaction time scales (τ < 10–30 ps) observed in trajectory calculations for low-energy DCl, CO_2, and CO projectiles colliding with an F-SAM surface.[7] Conversely, we can also invert this line of logic to infer that the lack of substantial thermal equilibration for the ν_2 =1 bend vibration suggests an upper-limit mean residence time of 100 ns for OCS in low-energy collisions at the gas–liquid interface.

Though such elementary predictions from inelastic Landau–Teller theory (plus semiclassical extensions by Rapp) are likely to fail quantitatively for such low collision probabilities, calculations in Figure 11 drive home a consistent message: even relatively low-energy vibrations (e.g., ν_2 = 520 cm^{-1}) in polyatomic molecules scattering from the gas–liquid interface remain largely in the vibrationally adiabatic limit and do not equilibrate with the surface temperature, at least for low-energy collisions predominantly sampling physisorbed regions of the surface potential. As a parting comment, we note that such residence times and perturbative nature of the collision dynamics will clearly be quite sensitive to the incident beam collision energy. For higher collision energies that sample further up on the repulsive wall, for example, one expects a significant increase in the effective repulsion parameter α and v_0, an even stronger decrease in the dimensionless $2\pi\omega/v_0\alpha$ exponent, and therefore exponential changes in vibrational excitation, deexcitation, and thermalization probabilities. On the other hand, higher-energy collisions might also encourage deeper penetration of the incident projectile into the liquid surface and thus open qualitatively different dynamical pathways for trapping-desorption (TD) vs impulsive scattering (IS) dynamics. Such studies of quantum-state-resolved OCS scattering at hyperthermal energies are currently underway, with which we hope to reveal new and unexpected insights into vibrational accommodation and equilibration dynamics at the gas–liquid interface.

V. SUMMARY AND CONCLUSIONS

In the present work, quantum-state-resolved collisional energy transfer of carbonyl sulfide (OCS) at the gas–liquid interface has been studied via molecular beam scattering and high-resolution IR spectroscopy, which has permitted identification of rotational, vibrational, and transverse Doppler excitation/accommodation of the projectile under low-incident-energy (E_{inc} = 2.2(4) kcal/mol) collision conditions. The results are found to be consistent with complete rotational and translational equilibration of the jet-cooled OCS (T_{rot} = 10 K) with the liquid surface over a variety of liquids (PFPE, squalene, and glycerol) and liquid temperatures (T_S = 263–303 K). By way of dramatic contrast, however, vibrational populations in the ground (00^00), ν_2 OCS bend (01^10), and ν_1 CS stretch (10^00) modes for the scattered OCS species remain far out of equilibrium with the liquid surface, indeed within experimental uncertainty at the same relative populations and vibrational temperatures observed in the incident OCS molecular beam. This observed propensity for vibrational adiabaticity and "spectator-like" behavior in the TD channel matches qualitative expectations from Fermi's golden rule, second-order perturbation theory, and well-established Landau–Teller/Rapp vibrational energy-transfer models. Furthermore,

https://doi.org/10.1021/acs.jpcc.1c05993
J. Phys. Chem. C 2021, 125, 22786–22796

the work points to obvious extensions into studies as a function of incident beam energy, for which the present analytical models predict contributions from polyatomic vibrational excitation, deexcitation, and equilibration dynamics under hyperthermal collision conditions. We are aware that the present study has barely touched the surface of this problem (quite literally!), but we hope that these first efforts provide the requisite stimulus for much needed additional theoretical and experimental work in this challenging but rapidly emerging area of gas−liquid collision dynamics.

AUTHOR INFORMATION

Corresponding Author

David J. Nesbitt − *JILA, National Institute of Standards and Technology and University of Colorado, Boulder, Colorado 80309, United States; Department of Physics and Department of Chemistry and Biochemistry, University of Colorado, Boulder, Colorado 80309, United States;* orcid.org/0000-0001-5365-1120; Email: djn@jila.colorado.edu

Author

Timothy A. Livingston Large − *JILA, National Institute of Standards and Technology and University of Colorado, Boulder, Colorado 80309, United States; Department of Physics, University of Colorado, Boulder, Colorado 80309, United States*

Complete contact information is available at: https://pubs.acs.org/10.1021/acs.jpcc.1c05993

Notes

The authors declare no competing financial interest.

ACKNOWLEDGMENTS

Funding for this work has been provided by the National Science Foundation under grant CHE-1665271 from the Chemical, Structure, Dynamics and Mechanisms-A Program, with early support for the QCL laser and initial apparatus construction from PHY-1734006 (Physics Frontier Center Program) and Air Force Office of Scientific Research (FA9550−15−1−0090).

REFERENCES

(1) Perkins, B. G.; Nesbitt, D. J. Quantum State-Resolved CO_2 Collisions at the Gas-Liquid Interface: Surface Temperature-Dependent Scattering Dynamics. *J. Phys. Chem. B* **2008**, *112*, 507−519.

(2) Perkins, B. G.; Nesbitt, D. J. Stereodynamics at the Gas-Liquid Interface: Orientation and Alignment of CO_2 Scattered from Perfluorinated Liquid Surfaces. *J. Phys. Chem. A* **2010**, *114*, 1398−1410.

(3) Faust, J. A.; Nathanson, G. M. Microjets and Coated Wheels: Versatile Tools for Exploring Collisions and Reactions at Gas-Liquid Interfaces. *Chem. Soc. Rev.* **2016**, *45*, 3609−3620.

(4) Tesa-Serrate, M. A.; Smoll, E. J.; Minton, T. K.; McKendrick, K. G. Atomic and Molecular Collisions at Liquid Surfaces. *Annu. Rev. Phys. Chem.* **2016**, *67*, 515−540.

(5) Waring, C.; King, K. L.; Bagot, P. A. J.; Costen, M. L.; McKendrick, K. G. Collision Dynamics and Reactive Uptake of OH Radicals at Liquid Surfaces of Atmospheric Interest. *Phys. Chem. Chem. Phys.* **2011**, *13*, 8457−8469.

(6) Hoffman, C. H.; Nesbitt, D. J. Quantum State Resolved 3D Velocity Map Imaging of Surface Scattered Molecules: Incident Energy Effects in HCl Plus Self-Assembled Monolayer Collisions. *J. Phys. Chem. C* **2016**, *120*, 16687−16698.

(7) Livingston Large, T. A.; Nesbitt, D. J. Low-Energy CO Scattering at the Gas-Liquid Interface: Experimental/Theoretical Evidence for a Novel Subthermal Impulsive Scattering (STIS) Channel. *J. Phys. Chem. C* **2020**, *124*, 28006−28017.

(8) Peng, Y.; Liu, L.; Cao, Z.; Li, S.; Mazyar, O. A.; Hase, W. L.; Yan, T. Chemical Dynamics Simulation of Ne Atom Scattering Off a Squalane Surface. *J. Phys. Chem. C* **2008**, *112*, 20340−20346.

(9) Bosio, S. B. M.; Hase, W. L. Energy Transfer in Rare Gas Collisions with Self-Assembled Monolayers. *J. Chem. Phys.* **1997**, *107*, 9677−9686.

(10) Perkins, B. G., Jr.; Nesbitt, D. J. High Resolution Dopplerimetry of Correlated Angular and Quantum State-Resolved CO_2 Scattering Dynamics at the Gas-Liquid Interface. *Phys. Chem. Chem. Phys.* **2010**, *12*, 14294−14308.

(11) Perkins, B. G.; Nesbitt, D. J. Toward Three-Dimensional Quantum State-Resolved Collision Dynamics at the Gas-Liquid Interface: Theoretical Investigation of Incident Angle. *J. Phys. Chem. A* **2009**, *113*, 4613−4625.

(12) Lenzer, T.; Luther, K.; Troe, J.; Gilbert, R. G.; Lim, K. F. Trajectory Simulations of Collisional Energy-Transfer in Highly Excited Benzene End Hexafluorobenzene. *J. Chem. Phys.* **1995**, *103*, 626−641.

(13) Moore, C. B. Vibration-Rotation Energy Transfer. *J. Chem. Phys.* **1965**, *43*, 2979.

(14) Barker, J. R.; Toselli, B. M. Infrared-Emission Studies of the Vibrational Deactivation of Benzene-Derivatives. *Int. Rev. Phys. Chem.* **1993**, *12*, 305−338.

(15) Rellergert, W. G.; Sullivan, S. T.; Schowalter, S. J.; Kotochigova, S.; Chen, K.; Hudson, E. R. Evidence for Sympathetic Vibrational Cooling of Translationally Cold Molecules. *Nature* **2013**, *495*, 490−494.

(16) Flynn, G. W.; Parmenter, C. S.; Wodtke, A. M. Vibrational Energy Transfer. *J. Phys. Chem. A* **1996**, *100*, 12817−12838.

(17) Nikitin, E. E.; Troe, J. 70 Years of Landau−Teller Theory for Collisional Energy Transfer. Semiclassical Three-Dimensional Generalizations of the Classical Collinear Model. *Phys. Chem. Chem. Phys.* **2008**, *10*, 1483−1501.

(18) Ewing, G. E. Selection-Rules for Vibrational-Energy Transfer - Vibrational Predissociation of Vanderwaals Molecules. *J. Phys. Chem. B* **1987**, *91*, 4662−4671.

(19) Kenyon, A. J.; McCaffery, A. J.; Quintella, C. M.; Zidan, M. D. Dynamics of the Gas-Liquid Interface from Laser Molecular-Beam Scattering. *Faraday Discuss.* **1993**, *96*, 245−254.

(20) Becker, C. H. An Experimental-Study of the Surface-Chemistry and Evaporation Kinetics of Liquid-Sodium. *Nucl. Instrum. Methods Phys. Res.* **1983**, *218*, 533−536.

(21) Becker, C. H. Laser and Ion-Beam Studies of Liquid-Sodium Surface-Chemistry and Na_2 Evaporation. *Surf. Sci.* **1985**, *149*, 67−80.

(22) Miksch, G.; Weber, H. G. Laser Diagnostics of Surface-Emitted Na_2 Molecules. *Chem. Phys. Lett.* **1982**, *87*, 544−547.

(23) Kenyon, A. J.; McCaffery, A. J.; Quintella, C. M.; Zidan, M. D. Liquid Surface Dynamics - a Quantum-Resolved Scattering Study. *Chem. Phys. Lett.* **1992**, *190*, 55−58.

(24) Jones, P. L.; Gaubatz, U.; Hefter, U.; Bergmann, K.; Wellegehausen, B. Optically Pumped Sodium-Dimer Supersonic-Beam Laser. *Appl. Phys. Lett.* **1983**, *42*, 222−224.

(25) Golibrzuch, K.; Shirhatti, P. R.; Altschaffel, J.; Rahinov, I.; Auerbach, D. J.; Wodtke, A. M.; Bartels, C. State-to-State Time-of-Flight Measurements of NO Scattering from Au(111): Direct Observation of Translation-to-Vibration Coupling in Electronically Nonadiabatic Energy Transfer. *J. Phys. Chem. A* **2013**, *117*, 8750−8760.

(26) Krüger, B. C.; Meyer, S.; Kandratsenka, A.; Wodtke, A. M.; Schafer, T. Vibrational Inelasticity of Highly Vibrationally Excited NO on Ag(111). *J. Phys. Chem. Lett.* **2016**, *7*, 441−446.

(27) Lau, J. A.; Schonemann, A. M.; Schwarzer, D.; Wodtke, A. M. The Coverage Dependence of the Infrared Absorption of CO Adsorbed to NaCl(100). *J. Chem. Phys.* **2020**, *153*, No. 154703.

(28) Shirhatti, P. R.; Rahinov, I.; Golibrzuch, K.; Werdecker, J.; Geweke, J.; Altschaffel, J.; Kumar, S.; Auerbach, D. J.; Bartels, C.; Wodtke, A. M. Observation of the Adsorption and Desorption of Vibrationally Excited Molecules on a Metal Surface. *Nat. Chem.* **2018**, *10*, 592−598.
(29) Steinsiek, C.; Shirhattii, P. R.; Geweke, J.; Lau, J. A.; Altschaffel, J.; Kandratsenka, A.; Bartels, C.; Wodtke, A. M. Translational Inelasticity of NO and CO in Scattering from Ultrathin Metallic Films of Ag/Au(111). *J. Phys. Chem. C* **2018**, *122*, 18942−18948.
(30) Wagner, R. J. V.; Henning, N.; Kruger, B. C.; Park, G. B.; Altschaffel, J.; Kandratsenka, A.; Wodtke, A. M.; Schafer, T. Vibrational Relaxation of Highly Vibrationally Excited CO Scattered from Au(111): Evidence for CO-Formation. *J. Phys. Chem. Lett.* **2017**, *8*, 4887−4892.
(31) Livingston Large, T. A.; Nesbitt, D. J. Quantum State and Doppler-Resolved Scattering of Thermal/Hyperthermal DCI at the Gas-Liquid Interface: Support for a Simple ″Lever Arm″ Model of the Energy-Transfer Dynamics (Vol 123, Pg 3449, 2019). *J. Phys. Chem. C* **2019**, *123*, 14104.
(32) Perkins, B. G.; Nesbitt, D. J. Correlated Angular and Quantum State-Resolved CO_2 Scattering Dynamics at the Gas-Liquid Interface. *J. Phys. Chem. A* **2008**, *112*, 9324−9335.
(33) Perkins, B. G.; Nesbitt, D. J. Quantum-State-Resolved CO_2 Scattering Dynamics at the Gas-Liquid Interface: Incident Collision Energy and Liquid Dependence. *J. Phys. Chem. B* **2006**, *110*, 17126−17137.
(34) Perkins, B. G.; Haber, T.; Nesbitt, D. J. Quantum State-Resolved Energy Transfer Dynamics at Gas-Liquid Interfaces: IR Laser Studies of CO_2 Scattering from Perfluorinated Liquids. *J. Phys. Chem. B* **2005**, *109*, 16396−16405.
(35) Gisler, A. W.; Nesbitt, D. J. On Probing Ions at the Gas-Liquid Interface by Quantum State-Resolved Molecular Beam Scattering: The Curious Incident of the Cation in the Night Time. *Faraday Discuss.* **2012**, *157*, 297−305.
(36) Proch, D.; Trickl, T. A High-Intensity Multi-Purpose Piezoelectric Pulsed Molecular-Beam Source. *Rev. Sci. Instrum.* **1989**, *60*, 713−716.
(37) Lednovich, S. L.; Fenn, J. B. Absolute Evaporation Rates for Some Polar and Nonpolar Liquids. *AIChE J.* **1977**, *23*, 454−459.
(38) Rothman, L. S.; Gamache, R. R.; Goldman, A.; Brown, L. R.; Toth, R. A.; Pickett, H. M.; Poynter, R. L.; Flaud, J. M.; Camypeyret, C.; Barbe, A.; et al. The Hitran Database - 1986 Edition. *Appl. Opt.* **1987**, *26*, 4058−4097.
(39) Ryazanov, M.; Nesbitt, D. J. Quantum-State-Resolved Studies of Aqueous Evaporation Dynamics: NO Ejection from a Liquid Water Microjet. *J. Chem. Phys.* **2019**, *150*, 044201.
(40) Tully, J. C. The Dynamics of Adsorption and Desorption. *Surf. Sci.* **1994**, *299−300*, 667−677.
(41) Landau, L. Theory of Sound Dispersion. *Phys. Z. Sowjetunion* **1936**, *10*, 34−43.
(42) Rapp, D. Complete Classical Theory of Vibrational Energy Exchange. *J. Chem. Phys.* **1960**, *32*, 735−737.

https://doi.org/10.1021/acs.jpcc.1c05993
J. Phys. Chem. C 2021, 125, 22786−22796